Dynamic equations for solid isotropic radially functionally graded circular cylinders

Citation for the original published paper (version of record):
Abadikhah, H., Folkow, P. (2018). Dynamic equations for solid isotropic radially functionally graded circular cylinders. Composite Structures, 195: 147-157.
http://dx.doi.org/10.1016/j.compstruct.2018.03.087

Dynamic equations for solid isotropic radially functionally graded circular cylinders

Hossein Abadikhah, Peter D. Folkow*

Department of Applied Mechanics, Chalmers University of Technology, SE-412 96 Göteborg, Sweden

Abstract

A hierarchy of dynamic equations for solid isotropic functionally graded circular cylinders is derived based on the three dimensional elastodynamic theory. The material parameters are assumed to vary in the radial direction. Using Fourier expansions in the circumferential direction and power series expansions in the radial direction, equations of motion are obtained for longitudinal, torsional, flexural and higher order motion to arbitrary Fourier and power orders. Numerical examples for eigenfrequencies and plots on mode shapes and stress distributions curves are presented for simply supported cylinders for different material distributions. The results illustrate that the present approach renders benchmark solutions provided higher order truncations are used, and act as engineering cylinder equations using low order truncation.

Keywords: Series expansion, Cylinder, Beam equation, Functionally graded, Eigenfrequency

1. Introduction

Functionally graded (FG) materials are non-homogeneous composites in which the properties change gradually in one or several directions. This continuous variation may be used as an alternative to laminated structures, and may thus eliminate the risk for delamination failures. The FG composites are usually made of a mixture of metal and ceramic phases, where the strength of the metal and the heat resistance of the ceramic make these materials popular in many different fields of engineering [1, 2].

The majority of work on FG structures considers basically two dimensional structures such as plates and shells, where the material parameters in most cases vary over the thickness. Of particular interest for the present work is the special case on FG cylindrical shells,

*Corresponding author. Tel: +46 31 7721521, Fax: +46 31 772 3827.
Email addresses: hossein.abadikhah@chalmers.se (Hossein Abadikhah), peter.folkow@chalmers.se (Peter D. Folkow)

where [3, 4, 5, 6] adopt classical, first and third order theories, while 3D based solutions are studied in [7, 8, 9, 10, 11]. Reviews on work for FGM shell structures are presented in [12, 13]

For structures such as flexural beams, torsional bars and longitudinal rods, the number of publications using functionally graded material properties is considerably lower compared to plates and shells. In the case of beams, there are some studies using statics [14, 15, 16], although most work consider dynamical effects. Here, analytical or semi analytical vibrational studies are presented in [17, 18, 19, 20, 21, 22, 23, 24] for Euler-Bernoulli, Timoshenko and higher order beam theories. Various numerical methods (finite element, meshless methods) have also bee adopted [25, 26, 27, 28, 29]. Among these works on beams only [15, 20] consider beams with circular cross section, while the rest deal with beams of rectangular cross section. In particular, vibrations of a Timoshenko like beam is studied in [20].

As for FG torsional bars and longitudinal rods with circular cross section, there seem to be only a few studies. Examples for torsional bars are [30, 31, 32, 33] for statics, while for axisymmetric rods one has [34, 35, 36, 37] considering various material configurations.

The present work on FG cylinders is an extension to earlier work adopting a power series approach for homogeneous cylinders [38, 40, 41]. The method is based on the three dimensional elastodynamic theory for a cylinder with radially varying material properties. Adopting Fourier series expansion in the circumferential direction and power series expansions of the displacement fields in the radial direction, sets of recursion relations are constructed for each Fourier mode. By using these recursion relations, all higher order displacement fields may be expressed in terms of the lowest order expansion functions without performing any truncations. This procedure is exact and may be performed to arbitrary order for each Fourier mode. By stating the radial boundary conditions on power series form, these boundary conditions represent sets of partial differential equations that constitute the complete set of cylinder equations. Using variational calculus, the end boundary conditions are obtained in an equally systematic manner. Hereby complete sets of cylinder equations may be derived to an (in principle) arbitrary order for the various Fourier modes (longitudinal, torsional, flexural, etc.). Higher order sets of time domain equations may be used for benchmark solutions to three dimensional FG cylinder problems, while lower order sets may be used as alternative engineering equations.

Numerical results are presented for simply supported cylinders for axisymmetric, torsional and flexural motion. The material distribution is assumed to vary using a power law in the radial direction. The results comprise eigenfrequencies and cross sectional fields using different truncation orders. Based on these results the low order cases may be used as approximate engineering FG cylinder theories while the higher order theories act as benchmark theories converging to the exact 3D solution.

2. Governing equations

Consider an isotropic and linearly elastic circular cylinder with radial coordinate r, circumferential coordinate θ and axial coordinate z. The corresponding radial, circumferential and longitudinal displacement fields are denoted by u, v and w. The cylinder is inhomogeneous where the material parameters may vary in the radial direction: density $\rho(r)$ and Lamé parameters $\lambda(r)$ and $\mu(r)$. The three dimensional elastodynamic cylinder equations are written

$$\begin{aligned}
&\frac{\partial \sigma_{rr}}{\partial r}+\frac{1}{r}\frac{\partial \sigma_{r\theta}}{\partial \theta}+\frac{\partial \sigma_{rz}}{\partial z}+\frac{\sigma_{rr}-\sigma_{\theta\theta}}{r}-\rho\frac{\partial^2 u}{\partial t^2}=0,\\
&\frac{\partial \sigma_{r\theta}}{\partial r}+\frac{1}{r}\frac{\partial \sigma_{\theta\theta}}{\partial \theta}+\frac{\partial \sigma_{\theta z}}{\partial z}+2\frac{\sigma_{r\theta}}{r}-\rho\frac{\partial^2 v}{\partial t^2}=0,\\
&\frac{\partial \sigma_{rz}}{\partial r}+\frac{1}{r}\frac{\partial \sigma_{\theta z}}{\partial \theta}+\frac{\partial \sigma_{zz}}{\partial z}+\frac{\sigma_{rz}}{r}-\rho\frac{\partial^2 w}{\partial t^2}=0,
\end{aligned} \tag{1}$$

where the stresses are

$$\begin{aligned}
&\sigma_{rr}=\lambda\left[\frac{1}{r}\frac{\partial}{\partial r}(ru)+\frac{1}{r}\frac{\partial v}{\partial \theta}+\frac{\partial w}{\partial z}\right]+2\mu\frac{\partial u}{\partial r},\\
&\sigma_{\theta\theta}=\lambda\left[\frac{1}{r}\frac{\partial}{\partial r}(ru)+\frac{1}{r}\frac{\partial v}{\partial \theta}+\frac{\partial w}{\partial z}\right]+2\mu\left[\frac{u}{r}+\frac{1}{r}\frac{\partial v}{\partial \theta}\right],\\
&\sigma_{zz}=\lambda\left[\frac{1}{r}\frac{\partial}{\partial r}(ru)+\frac{1}{r}\frac{\partial v}{\partial \theta}+\frac{\partial w}{\partial z}\right]+2\mu\frac{\partial w}{\partial z},\\
&\sigma_{r\theta}=\mu\left[\frac{1}{r}\frac{\partial u}{\partial \theta}+\frac{\partial v}{\partial r}-\frac{v}{r}\right],\qquad \sigma_{rz}=\mu\left[\frac{\partial u}{\partial z}+\frac{\partial w}{\partial r}\right],\qquad \sigma_{\theta z}=\mu\left[\frac{\partial v}{\partial z}+\frac{1}{r}\frac{\partial w}{\partial \theta}\right].
\end{aligned} \tag{2}$$

3. Series expansion and recursion relations

In order to derive sets of partial differential equations for FG cylinders, the displacement fields are expanded in both the radial and the circumferential directions. In the latter case, consider Fourier series expansion as

$$u=\sum_{m=0}^{\infty}\tilde{u}_m(r,z,t)\cos m\theta,\qquad v=\sum_{m=0}^{\infty}\tilde{v}_m(r,z,t)\sin m\theta,\qquad w=\sum_{m=0}^{\infty}\tilde{w}_m(r,z,t)\cos m\theta, \tag{3}$$

where the angle θ is measured from a vertical axis in a plane through the cross section of the cylinder with a horizontal axis, as defined in [39]. Consequently, the case $m=0$ corresponds to the axisymmetric motion with coupled radial and longitudinal displacements, u and w respectively. For all modes $m>0$ there are coupling among the three fields. Of particular interest is the case $m=1$ for flexural motion in the vertical direction. By interchanging $\cos m\theta$ and $\sin m\theta$ in Eq. (3), purely torsional motion v is stated for $m=0$.

In the radial direction the displacement terms are expanded in power series. The Fourier expanded displacements fields may be written according to

$$\begin{aligned}
\tilde{u}_m(r,z,t) &= \sum_{k=0}^{\infty} r^{m+k-1} u_{m+k-1,m}(z,t), \\
\tilde{v}_m(r,z,t) &= \sum_{k=0}^{\infty} r^{m+k-1} v_{m+k-1,m}(z,t), \\
\tilde{w}_m(r,z,t) &= \sum_{k=0}^{\infty} r^{m+k} w_{m+k,m}(z,t),
\end{aligned} \tag{4}$$

where the indexes are such that for $u_{k,m}(z,t)$, k connects to the radial expansion order, while m connects to the circumferential Fourier expansion order.

Here the construction of the radial power series indexes are based on the relation [41]

$$u_{k,m} = v_{k,m} = w_{k,m-1} \equiv 0, \qquad k < m-1. \tag{5}$$

which becomes apparent from the recursion relations Eqs. (14)–(16).

As for the radially varying material parameters, it is assumed that these may be expanded in Taylor series

$$f(r) = \sum_{k=0}^{\infty} r^k f_k, \tag{6}$$

where f covers the parameters $\{\rho, \lambda, \mu\}$, see more in Section 5.1.

The expressions for the stresses follow directly from Eq. (2) using Eq. (4) and Eq. (6). Hereby $\{\sigma_{rr}, \sigma_{\theta\theta}, \sigma_{zz}, \sigma_{rz}\}$ are expanded in $\cos m\theta$ and $\{\sigma_{r\theta}, \sigma_{\theta z}\}$ are expanded in $\sin m\theta$. Hence the stresses may be written

$$\sigma_{ij} = \sum_{m=0}^{\infty} \tilde{\sigma}_{ij,m}(r,z,t)\{\cos m\theta; \sin m\theta\}, \tag{7}$$

using either $\cos m\theta$ or $\sin m\theta$ according to above. The Fourier modes become

$$\tilde{\sigma}_{rr,m} = \sum_{k=0}^{\infty}\sum_{p=0}^{k}\big([(m+p)(\lambda_{k-p}+2\mu_{k-p})-2\mu_{k-p}]u_{m+p-1,m}+ \\ +m\lambda_{k-p}v_{m+p-1,m}+\lambda_{k-p}w'_{m+p-2,m}\big)r^{m+k-2}, \tag{8}$$

$$\tilde{\sigma}_{\theta\theta,m} = \sum_{k=0}^{\infty}\sum_{p=0}^{k}\big([(m+p)\lambda_{k-p}+2\mu_{k-p}]u_{m+p-1,m}+ \\ +m(\lambda_{k-p}+2\mu_{k-p})v_{m+p-1,m}+\lambda_{k-p}w'_{m+p-2,m}\big)r^{m+k-2}, \tag{9}$$

$$\tilde{\sigma}_{zz,m} = \sum_{k=0}^{\infty}\sum_{p=0}^{k}\big((m+p)\lambda_{k-p}u_{m+p-1,m}+m\lambda_{k-p}v_{m+p-1,m}+ \\ +(\lambda_{k-p}+2\mu_{k-p})w'_{m+p-2,m}\big)r^{m+k-2}, \tag{10}$$

$$\tilde{\sigma}_{r\theta,m} = \sum_{k=0}^{\infty}\sum_{p=0}^{k}\mu_{k-p}\big((m+p-2)v_{m+p-1,m}-mu_{m+p-1,m}\big)r^{m+k-2}, \tag{11}$$

$$\tilde{\sigma}_{rz,m} = \sum_{k=0}^{\infty}\sum_{p=1}^{k+1}\mu_{k-p+1}\big(u'_{m+p-2,m}-(m+p-1)w_{m+p-1,m}\big)r^{m+k-1}, \tag{12}$$

$$\tilde{\sigma}_{\theta z,m} = \sum_{k=0}^{\infty}\sum_{p=1}^{k+1}\mu_{k-p+1}\big(v'_{m+p-2,m}-mw_{m+p-1,m}\big)r^{m+k-1}, \tag{13}$$

where a prime denotes a z-derivative. The stress terms with negative powers of r appearing for $m = 0$ and $m = 1$ may be shown to be zero from the recursion relations below Eqs. (14)–(16) in line with [41].

Insertion of the stress series expansions Eqs. (8)–(13) and the displacement series Eq. (4) together with the density series Eq. (6) into the governing equations of motion Eq. (1) gives power series expansion equations in the radial coordinate r for each Fourier mode m. By collecting equal powers of r, the solution of the equation system for each power yields

the recursion formulas

$$\sum_{p=0}^{k}\Bigg(\big[(m+k-2)(m+p)(\lambda_{k-p}+2\mu_{k-p})-(2k-2p+m^2)\mu_{k-p}\big]u_{m+p-1,m}+ \\ m\big[(m+k-2)\lambda_{k-p}+(m+p-4)\mu_{k-p}\big]v_{m+p-1,m}+(m+k-2)\lambda_{k-p}w'_{m+p-2,m}+ \\ (m+p)\mu_{k-p-2}w'_{m+p,m}+\mu_{k-p-2}u''_{m+p-1,m}-\rho_{k-p-2}\ddot{u}_{m+p-1,m}\Bigg)=0, \tag{14}$$

$$\sum_{p=0}^{k}\Bigg(\big[(m+k)(m+p-2)\mu_{k-p}-m^2(\lambda_{k-p}+2\mu_{k-p})\big]v_{m+p-1,m}- \\ m\big[(m+p)\lambda_{k-p}+(m+k+2)\mu_{k-p}\big]u_{m+p-1,m}-m\lambda_{k-p}w'_{m+p-2,m}- \\ m\mu_{k-p-2}w'_{m+p,m}+\mu_{k-p-2}v''_{m+p-1,m}-\rho_{k-p-2}\ddot{v}_{m+p-1,m}\Bigg)=0, \tag{15}$$

$$\sum_{p=0}^{k}\Bigg(\big[(m+p)\lambda_{k-p}+(m+k)\mu_{k-p}\big]u'_{m+p-1,m}+ \\ m(\lambda_{k-p}+\mu_{k-p})v'_{m+p-1,m}+\big[(m+k)(m+p)-m^2\big]\mu_{k-p}w_{m+p,m}+ \\ (\lambda_{k-p}+2\mu_{k-p})w''_{m+p-2,m}-\rho_{k-p}\ddot{w}_{m+p-2,m}\Bigg)=0, \tag{16}$$

for $k=0,1,\ldots$. Hence, for each specific $k>0$ these recursion relations make it possible to express the higher order fields $u_{m+k-1,m}$ and $v_{m+k-1,m}$ from Eqs. (14)–(15) and $w_{m+k,m}$ from Eq. (16) in terms of lower order displacement fields and derivatives thereof. The procedure follow from rewriting Eqs. (14)–(16) as

$$a_1\,u_{m+k-1,m}+a_2\,v_{m+k-1,m}=f_u\left(u_{m+p-2,m},v_{m+p-2,m},w'_{m+p-2,m},u''_{m+p-3,m},\ddot{u}_{m+p-3,m}\right) \tag{17}$$

$$a_3\,u_{m+k-1,m}+a_4\,v_{m+k-1,m}=f_v\left(u_{m+p-2,m},v_{m+p-2,m},w'_{m+p-2,m},v''_{m+p-3,m},\ddot{v}_{m+p-3,m}\right) \tag{18}$$

$$a_5\,w_{m+k,m}=f_w\left(w_{m+p-1,m},u'_{m+p-1,m},v'_{m+p-1,m},w''_{m+p-2,m},\ddot{w}_{m+p-2,m}\right) \tag{19}$$

for $p=0,1,\ldots,k$ using that a_i are functions of $\{k,m,\lambda_0,\mu_0\}$. Here all negative powers of the material parameters have been disregarded according to Eq. (6).

The case $k=0$ is trivially fulfilled for these equations using Eq. (5) provided that

$$u_{m-1,m}+v_{m-1,m}=0. \tag{20}$$

This constraint was also reported for the homogeneous rod [41].

Proceeding for $k\geq 1$ by first solving Eqs. (17)–(18) and then considering Eq. (19) for each k, the fields $\{u_{m+k-1,m},v_{m+k-1,m},w_{m+k,m}\}$ are expressed in the lowest order independent fields $\{u_{m-1,m},v_{m,m},w_{m,m}\}$ in a fashion similar to [41].

4. Hierarchies of FG cylinder equations and boundary conditions

This section aims at deriving the dynamical cylinder equations through the lateral boundary conditions and the pertinent end boundary conditions.

4.1. Dynamic cylinder equations

Consider a cylinder of length L and radius a. At each point on the lateral surface $r = a$, either the displacement or the traction is to be prescribed in each coordinate direction. These given fields are denoted by $\{\hat{u}_r, \hat{u}_\theta, \hat{u}_z\}$ and $\{\hat{t}_r, \hat{t}_\theta, \hat{t}_z\}$, respectively. Performing a Fourier series expansion for each term reads

$$\hat{u}_i(\theta, z, t) = \sum_{m=0}^{\infty} \hat{u}_{i,m}(z, t)\{\cos m\theta; \sin m\theta\}, \quad \hat{t}_i(\theta, z, t) = \sum_{m=0}^{\infty} \hat{t}_{i,m}(z, t)\{\cos m\theta; \sin m\theta\}, \tag{21}$$

using either $\cos m\theta$ or $\sin m\theta$ according to Eq. (3) and Eq. (7). So by using Eq. (3) at the lateral boundary, the displacement boundary conditions for each m become

$$\tilde{u}_m(a, z, t) = \hat{u}_{r,m}(z, t), \quad \tilde{v}_m(a, z, t) = \hat{u}_{\theta,m}(z, t), \quad \tilde{w}_m(a, z, t) = \hat{u}_{z,m}(z, t), \tag{22}$$

adopting the series ansatz Eq. (4). Similarly, for the stresses using Eq. (7) the traction boundary conditions for each m become

$$\tilde{\sigma}_{rr,m}(a, z, t) = \hat{t}_{r,m}(z, t), \quad \tilde{\sigma}_{r\theta,m}(a, z, t) = \hat{t}_{\theta,m}(z, t), \quad \tilde{\sigma}_{rz,m}(a, z, t)) = \hat{t}_{z,m}(z, t), \tag{23}$$

adopting the series ansatz Eqs. (8), (11) and (12) respectively.

These lateral boundary conditions (22)–(23) constitute for each z a set of partial differential cylinder equations of motion that may be truncated to any order. Hence, by stating one of the fields for each of the three pairs $\{\hat{t}_r, \hat{u}_r\}, \{\hat{t}_\theta, \hat{u}_\theta\}, \{\hat{t}_z, \hat{u}_z\}$ along the lateral surface, a set of three equations forming a hierarchy of approximate cylinder equations is obtained. Adopting the recursion relations (14)–(16), these cylinder equations are expressed as a set of equations in terms of the mutually independent lowest order index terms.

4.2. End conditions

Consider prescribed end conditions where either displacements $\{\hat{u}_r, \hat{u}_\theta, \hat{u}_z\}$ or tractions $\{\hat{t}_r, \hat{t}_\theta, \hat{t}_z\}$ or combinations thereof are to be stated on $z = \{0, L\}$. Variationally consistent end boundary conditions are obtained adopting a generalized Hamilton principle described previously for homogeneous cylinders in [40, 41]. The method is based on stating virtual

displacements and tractions, and using integrations over the end cross sections for each Fourier mode as

$$\int (\hat{u}_{r,m} - \tilde{u}_m)\, \delta\tilde{\sigma}_{rz,m}\, r\mathrm{d}r = \int (\hat{u}_{\theta,m} - \tilde{v}_m)\, \delta\tilde{\sigma}_{\theta z,m}\, r\mathrm{d}r = \int (\hat{u}_{z,m} - \tilde{w}_m)\, \delta\tilde{\sigma}_{zz,m}\, r\mathrm{d}r = 0, \tag{24}$$

$$\int \left(\hat{t}_{r,m} \pm \tilde{\sigma}_{rz,m}\right) \delta\tilde{u}_m\, r\mathrm{d}r = \int \left(\hat{t}_{\theta,m} \pm \tilde{\sigma}_{\theta z,m}\right) \delta\tilde{v}_m\, r\mathrm{d}r = \int \left(\hat{t}_{z,m} \pm \tilde{\sigma}_{zz,m}\right) \delta\tilde{w}_m\, r\mathrm{d}r = 0, \tag{25}$$

where the notation $\pm$ in (25) refers to the left/right end. Here the Fourier mode notation as in (21) has essentially been adopted, but now with $\hat{u}_{i,m}(r,t)$ and $\tilde{u}_m(r,z,t)$ etc. on $z = \{0, L\}$. By applying the power series expansions for the displacements Eq. (4) and the stresses Eqs. (10), (12) and (13), three sets of equations at each end are to be solved from Eqs. (24)–(25).

In order to illustrate the end condition procedures, consider prescribed normal traction $\hat{t}_{z,m}$ at $z = L$. To this end, introduce the notation for the stress $\tilde{\sigma}_{zz,m}(r,L,t)$ in Eq. (10) as

$$\tilde{\sigma}_{zz,m}(r,L,t) = \sum_{k=0}^{\infty} \sigma_{zz,\{m,k\}}(L,t) r^{m+k-2}. \tag{26}$$

Using this together with Eq. (4) for the $\tilde{w}_m$ field in the last integral in Eq. (25) results in

$$\int_0^a \left(\hat{t}_{z,m}(r,t) - \sum_{i=0}^{\infty} r^{m+i-2} \sigma_{zz,\{m,i\}}(L,t)\right) \left(\sum_{j=0}^{\infty} r^{m+j} \delta w_{m+j,m}(L,t)\right) r\,\mathrm{d}r = 0. \tag{27}$$

By performing the radial integration for each independent virtual displacement $\delta w_{m+j,m}$, the resulting equation system may be solved for every $\sigma_{zz,\{m,i\}}$ term. More specifically, assuming truncation order N gives

$$\int_0^a \left(\hat{t}_{z,m}(r,t) - \sum_{i=0}^{N} r^{m+i-2} \sigma_{zz,\{m,i\}}(L,t)\right) r^{m+1+j}\,\mathrm{d}r = 0, \quad j = 0, 1, \cdots, N, \tag{28}$$

where it is straightforward to derive the $N+1$ boundary fields $\sigma_{zz,\{m,i\}}(L,t)$, $(i = 0, 1, \cdots, N)$, from the $N+1$ integrals in Eq. (28). In the special case of $m = 0$ one obtains $N-1$ stress terms $\sigma_{zz,\{0,i\}}(L,t)$ for j up to $N-2$, while $m = 1$ renders N stress terms $\sigma_{zz,\{1,i\}}(L,t)$ for j up to $N-1$ since the singular terms $\sigma_{zz,\{0,0\}} = \sigma_{zz,\{0,1\}} = \sigma_{zz,\{1,0\}} = 0$ from the recursion relations. Note that the homogeneous boundary case $\hat{t}_{z,m}(r,t) = 0$ results in $\sigma_{zz,\{m,i\}}(L,t) = 0$ for all i. These boundary stress fields are then expressed in the displacement terms of various orders appearing in Eq. (10), which in turn may be written in the lowest order displacement fields adopting the recursion relations Eqs. (14)–(16). The other possible stress and displacement boundary cases are treated in an analogous way.

Consequently, by adopting this procedure a wide range of end boundary conditions, both homogeneous and non-homogeneous, may be studied. Of particular interest is the standard cases such as free or clamped ends. Following the procedure outlined above, the series terms for a free end at $z = L$ become $\sigma_{rz,\{m,i\}}(L,t) = \sigma_{\theta z,\{m,i\}}(L,t) = \sigma_{zz,\{m,i\}}(L,t) = 0$ for all i. Similarly, a clamped end at $z = L$ becomes $u_{m+i-1,m}(L,t) = v_{m+i-1,m}(L,t) = w_{m+i,m}(L,t) = 0$ for all i.

5. Numerical results

In order to illustrate the present method applied to vibrational problems on FG cylinders, eigenfrequencies and eigenmodes are to be calculated varying the truncation order N for different geometries and material distributions for torsional, axisymmetric and flexural motion. Consider only the standard case of free lateral surface, that is the prescribed fields $\hat{t}_{r,m}(z,t) = \hat{t}_{\theta,m}(z,t) = \hat{t}_{z,m}(z,t) = 0$ resulting in $\tilde{\sigma}_{rr,m}(a,z,t) = \tilde{\sigma}_{r\theta,m}(a,z,t) = \tilde{\sigma}_{rz,m}(a,z,t) = 0$ from Eq. (23). Consequently, the cylinder equations of motion for a fixed m are obtained through the three partial differential equations Eqs. (8), (11) and (12) at $r = a$, together with the recursion relations Eqs. (14)–(16).

As for the end boundary conditions, consider only mixed boundary conditions (simply supported), that is the prescribed fields $\hat{u}_{r,m}(r,t) = \hat{v}_{r,m}(r,t) = 0$ and $\hat{t}_{z,m}(r,t) = 0$ on $z = \{0, L\}$. Using the procedures stated in Section 4.2, this results in homogeneous series expansion terms $u_{m+i-1,m}(z,t) = v_{m+i-1,m}(z,t) = 0$ and $\sigma_{zz,\{m,i\}}(z,t) = 0$ for all i on $z = \{0, L\}$. It should be noted that it is possible to handle other boundary conditions numerically, e.g. free or clamped ends [41], albeit the simply supported case is the simplest.

5.1. Material parameters

The are several micromechanics models for various FG materials constitutions that have been developed. In the present work consider a two-phase composite where the cylinder core is of aluminum while the ceramic lateral surface acts as a thermal barrier made of silicon carbide [42]. The material constants for aluminum are $E_a = 70$ GPa, $\nu_a = 0.3$, $\rho_a = 2702$ kg/m^3 while one has for silicon carbide $E_c = 427$ GPa, $\nu_c = 0.17$, $\rho_c = 3100$ kg/m^3. These properties are related to the Lamé parameters through $\lambda_i = E_i\nu_i/(1+\nu_i)(1-2\nu_i)$ and $\mu_i = E_i/2(1+\nu_i)$ for $i = \{a, c\}$. The material distribution in the radial direction follows the power law, and the ceramic phase varies as

$$V_c(r) = (r/a)^p\,, \tag{29}$$

where the power index p is a positive number. Note that the volume fraction law reads $V_a + V_c = 1$. Hence, for $p = 0$ the cylinder consists of pure ceramic, and the metal influence increases as p increases. The effective mass density is assumed to be modeled

using the Voigt model $\rho(r) = \rho_a V_a(r) + \rho_c V_c(r)$, while the Lamé parameters follow from the Mori-Takana model [43]

$$\frac{K(r) - K_a}{K_c - K_a} = \frac{V_c(r)}{1 + V_a(r)\,(3(K_c - K_a)/(3K_a + \mu_a))}, \tag{30}$$

$$\frac{\mu(r) - \mu_a}{\mu_c - \mu_a} = \frac{V_c(r)}{1 + V_a(r)(\mu_c - \mu_a)/(\mu_a + f_a)}, \qquad f_a = \frac{\mu_a(9K_a + 8\mu_a)}{6(K_a + 2\mu_a)}. \tag{31}$$

where $K = \lambda + 2\mu/3$ is the bulk modulus.

Hereby, it is straightforward for the cases studied below to expand the material fields $\rho(r), \lambda(r)$ and $\mu(r)$ in radial Taylor series in line with Eq. (6).

5.2. Torsional mode, $m = 0$

For the purely torsional case, the circumferential displacement field is uncoupled from the other two displacement fields. From Eqs. (3)–(4) the displacement becomes

$$v(r, \theta, z, t) = \sum_{k=0}^{\infty} r^k v_{k,0}(z, t), \tag{32}$$

and is thus independent of the circumferential angle θ. The single cylinder equation of motion is obtained from the free lateral surface condition $\tilde{\sigma}_{r\theta,0}(a, z, t) = 0$ in Eq. (11). Since the recursion relation Eq. (15) shows that $v_{0,0} = 0$, Eq. (11) reduces to

$$\sum_{p=0}^{k} \left((k+2)p\,\mu_{k-p}\,v_{p+1,0} + \mu_{k-p-2}\,v''_{p+1,0} - \rho_{k-p-2}\,\ddot{v}_{p+1,0} \right) = 0, \tag{33}$$

for $k = 0, 1, \ldots$. Hence, all higher order fields may be expressed in terms of $v_{1,0}$ and derivatives thereof. The end boundary conditions become $v_{i+1,0}(z, t) = 0$ for all i on $z = \{0, L\}$.

Consider the three lowest eigenfrequencies for two different cylinder lengths; $L/a = 20$ and $L/a = 10$. The results are for various power indexes p and truncations orders N as noted in Tables 1 and 2 using the non dimensional frequency $\Omega_n = \omega_n a/c_c$, where the velocity c_c is for the ceramic silicon carbide defined as $c_c = \sqrt{E_c/\rho_c}$.

It is clear from these two tables that rather high truncation orders are needed to render accurate results; this differ considerably from the homogeneous case where accurate results are obtained already for the first few truncations orders [41]. As the power order p is increased, more terms are needed to render accurate results due to the more complex material variation. It is interesting to note to what extent the higher power orders p influence the eigenfrequencies for the lower order truncations. Clearly, the truncation order must reach a certain level so that the effects from the power orders p are displayed in the equations of motion.

	$N=2$	$N=3$	$N=4$	$N=5$	$N=6$	$N=10$	$N=15$	$N=25$	$N=35$	$N=50$	$N=70$	$N=90$	$N=110$	$N=130$	$N=150$
$p=1$															
Ω_1	0.042209	0.059691	0.069097	0.074247	0.077514	0.082240	0.083264	0.083452	0.083458	0.083458	0.083458	0.083458	0.083458	0.083458	0.083458
Ω_2	0.084418	0.11938	0.13860	0.14817	0.15513	0.16448	0.16650	0.16688	0.16689	0.16689	0.16689	0.16689	0.16689	0.16689	0.16689
Ω_3	0.12663	0.17907	0.20899	0.22144	0.23293	0.24671	0.24970	0.25027	0.25029	0.25029	0.25029	0.25029	0.25029	0.25029	0.25029
$p=2$															
Ω_1	0.042209	0.042209	0.057400	0.057400	0.064861	0.071244	0.073591	0.075104	0.075316	0.075354	0.075357	0.075357	0.075357	0.075357	0.075357
Ω_2	0.084418	0.084418	0.11493	0.11493	0.12959	0.14243	0.14714	0.15018	0.15060	0.15068	0.15068	0.15068	0.15068	0.15068	0.15068
Ω_3	0.12663	0.12663	0.17272	0.17272	0.19405	0.21348	0.22060	0.22519	0.22582	0.22593	0.22594	0.22594	0.22594	0.22594	0.22594
$p=3$															
Ω_1	0.042209	0.042209	0.042209	0.055631	0.055631	0.061935	0.067118	0.069426	0.070138	0.070299	0.070325	0.070329	0.070329	0.070329	0.070329
Ω_2	0.084418	0.084418	0.084418	0.11136	0.11136	0.12385	0.13420	0.13881	0.14024	0.14056	0.14061	0.14062	0.14062	0.14062	0.14062
Ω_3	0.12663	0.12663	0.12663	0.16730	0.16730	0.18573	0.20121	0.20812	0.21028	0.21075	0.21083	0.21084	0.21084	0.21084	0.21084
$p=5$															
Ω_1	0.042209	0.042209	0.042209	0.042209	0.042209	0.053090	0.057957	0.061808	0.063145	0.063818	0.064042	0.064090	0.064101	0.064103	0.064104
Ω_2	0.084418	0.084418	0.084418	0.084418	0.084418	0.10614	0.11589	0.12359	0.12626	0.12760	0.12805	0.12814	0.12816	0.12817	0.12817
Ω_3	0.12663	0.12663	0.12663	0.12663	0.12663	0.15910	0.17379	0.18530	0.18930	0.19131	0.19198	0.19212	0.19215	0.19216	0.19216

Table 1: Torsional mode, $L/a = 20$.

	$N=2$	$N=3$	$N=4$	$N=5$	$N=6$	$N=10$	$N=15$	$N=25$	$N=35$	$N=50$	$N=70$	$N=90$	$N=110$	$N=130$	$N=150$	$N=170$
$p=1$																
Ω_1	0.084418	0.11938	0.13860	0.14817	0.15513	0.16448	0.16650	0.16688	0.16689	0.16689	0.16689	0.16689	0.16689	0.16689	0.16689	0.16689
Ω_2	0.16884	0.23876	0.28083	0.29374	0.31095	0.32887	0.33283	0.33360	0.33362	0.33362	0.33362	0.33362	0.33362	0.33362	0.33362	0.33362
Ω_3	0.25325	0.35814	0.43267	0.43427	0.46734	0.49255	0.49885	0.49997	0.50000	0.50000	0.50000	0.50000	0.50000	0.50000	0.50000	0.50000
$p=2$																
Ω_1	0.084418	0.084418	0.11493	0.11493	0.12959	0.14243	0.14714	0.15018	0.15060	0.15068	0.15068	0.15068	0.15068	0.15068	0.15068	0.15068
Ω_2	0.16884	0.16884	0.23092	0.23092	0.25808	0.28431	0.29391	0.30012	0.30093	0.30109	0.30110	0.30110	0.30110	0.30110	0.30110	0.30110
Ω_3	0.25325	0.25325	0.34936	0.34936	0.38417	0.4248	0.43978	0.44961	0.45073	0.45097	0.45099	0.45099	0.45099	0.45099	0.45099	0.45099
$p=3$																
Ω_1	0.084418	0.084418	0.084418	0.11136	0.11136	0.12385	0.13420	0.13881	0.14024	0.14056	0.14061	0.14062	0.14062	0.14062	0.14062	0.14062
Ω_2	0.16884	0.16884	0.16884	0.22356	0.22355	0.24757	0.26813	0.27731	0.28020	0.28083	0.28093	0.28095	0.28095	0.28095	0.28095	0.28095
Ω_3	0.25325	0.25325	0.25325	0.33764	0.33754	0.37113	0.40156	0.41513	0.41960	0.42049	0.42065	0.42067	0.42067	0.42067	0.42067	0.42067
$p=5$																
Ω_1	0.084418	0.084418	0.084418	0.084418	0.084418	0.10614	0.11589	0.12359	0.12626	0.12760	0.12805	0.12814	0.12816	0.12817	0.12817	0.12817
Ω_2	0.16884	0.16884	0.16884	0.16884	0.16884	0.21194	0.23163	0.24693	0.25224	0.25491	0.25580	0.25599	0.25603	0.25604	0.25605	0.25605
Ω_3	0.25325	0.25325	0.25325	0.25325	0.25325	0.31705	0.34706	0.36980	0.37768	0.38161	0.38295	0.38323	0.38330	0.38331	0.38332	0.38332

Table 2: Torsional mode $L/a = 10$.

The differences among the truncations for the lowest eigenmode may be illustrated by studying the mode shapes and stress distributions over the cross section at $z = L/2$ for the $p = 5$ case. The eigenmodes are normalized so that the maximal displacement v is equal to unity at $r = a$ and $z = L/2$.

The differences among the truncation orders are very small for the displacement v, where the displacement increases almost linearly with increasing radius in all cases; this result is not displayed here. As for the stress distributions, the shear stresses are presented in Figure 1. It is seen that the truncation orders affect the accuracies; in Figure 1(a) most notably at the peak level, while in Figure 1(b) as approaching the surface. Note in Figure 1(a) that the lowest presented order $N = 5$ is close to zero for all r, and that the free surface boundary condition is fulfilled for all orders.

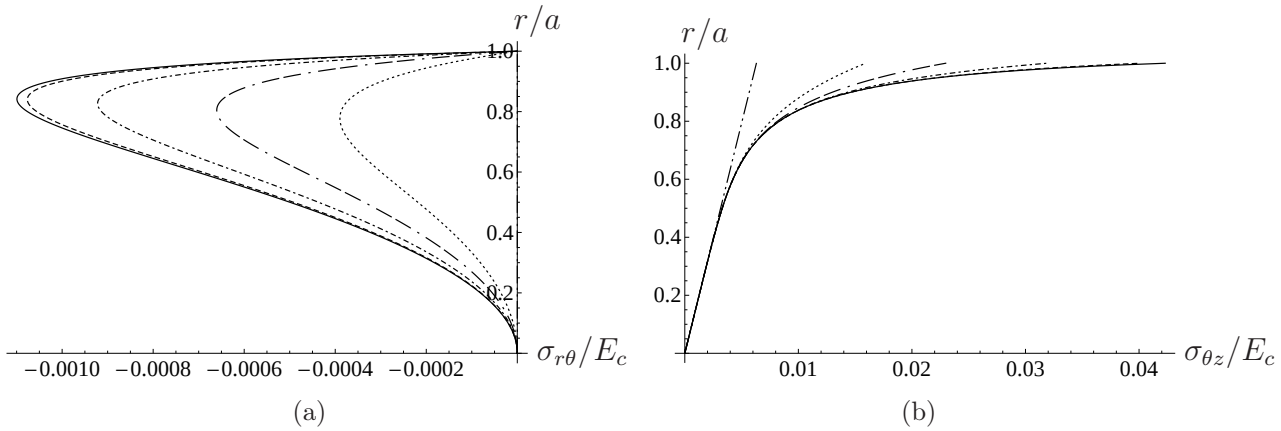

Figure 1: Shear stresses $\sigma_{r\theta}$ (a) and $\sigma_{\theta z}$ (b) for the first torsional mode with $p = 5$: —— $N = 150$, - - - $N = 50$, -·- $N = 25$, – – · – – $N = 15$, · · · $N = 10$, – · · – $N = 5$.

5.3. Axisymmetric mode, $m = 0$

For the purely axisymmetric case, there is a coupling between the radial and longitudinal displacement fields. From Eqs. (3)–(4) the two displacements become

$$\begin{aligned} u(r,\theta,z,t) &= \sum_{k=0}^{\infty} r^k u_{k,0}(z,t), \\ w(r,\theta,z,t) &= \sum_{k=0}^{\infty} r^k w_{k,0}(z,t), \end{aligned} \tag{34}$$

and thus independent of the circumferential angle θ. The coupled cylinder equations of motion are $\tilde{\sigma}_{rr,0}(a,z,t) = \tilde{\sigma}_{rz,0}(a,z,t) = 0$ from Eqs. (8) and (12) together with the recursion relations Eqs. (14) and (16). From Eq. (14) it is seen that $u_{0,0} = 0$ which causes all higher order fields to be expressed in terms $u_{1,0}$ and $w_{0,0}$ and derivatives thereof. The simply supported end boundary conditions become $u_{i+1,0}(z,t) = 0$ and $\sigma_{zz,\{0,i\}}(z,t) = 0$ for all i on $z = \{0, L\}$.

As for the torsional case, the three lowest eigenfrequencies for various power indexes p and truncations orders N using the length to radius relation $L/a = 20$ and $L/a = 10$ are presented in Tables 3 and 4.

The convergence rate resembles the torsional case, where the eigenfrequencies are slightly higher for the axisymmetric case as expected [40, 41]. The pattern that a certain truncation order is needed in order to influence the eigenfrequencies as the power order p is increased is also seen here. It is surprising that the convergence error when increasing the power order N does not always decrease in a monotonic manner as for the torsional case. This effect is seen for the second and third eigenfrequencies, especially for the less slender cylinder $L/a = 10$ in the vicinity of $N = 6$. Note that contrary to all the other cases, the third eigenfrequency for $p = 1$ and $N = 3$ marked by * in Table 4 has an imaginary part that is

	$N=2$	$N=3$	$N=4$	$N=5$	$N=6$	$N=10$	$N=15$	$N=25$	$N=35$	$N=50$	$N=70$	$N=90$	$N=110$	$N=130$	$N=150$
$p=1$															
Ω_1	0.091487	0.10303	0.10840	0.11203	0.11389	0.11679	0.11736	0.11745	0.11745	0.11745	0.11745	0.11745	0.11745	0.11745	0.11745
Ω_2	0.18244	0.20782	0.21520	0.22398	0.22692	0.23288	0.23403	0.23421	0.23421	0.23421	0.23421	0.23421	0.23421	0.23421	0.23421
Ω_3	0.27223	0.31716	0.31894	0.33528	0.33864	0.34755	0.34922	0.34947	0.34948	0.34948	0.34948	0.34948	0.34948	0.34948	0.34948
$p=2$															
Ω_1	0.068455	0.086551	0.086761	0.094582	0.094699	0.10111	0.10376	0.10458	0.10469	0.10470	0.10470	0.10470	0.10470	0.10470	0.10470
Ω_2	0.13661	0.17339	0.17398	0.18825	0.18852	0.20143	0.20677	0.20835	0.20857	0.20860	0.20860	0.20860	0.20860	0.20860	0.20860
Ω_3	0.20415	0.26090	0.26233	0.27997	0.28041	0.29999	0.30823	0.31041	0.31074	0.31079	0.31079	0.31079	0.31079	0.31079	0.31079
$p=3$															
Ω_1	0.068001	0.068396	0.08336	0.083374	0.083394	0.093055	0.094838	0.097082	0.097412	0.097531	0.097550	0.097552	0.097552	0.097552	0.097552
Ω_2	0.13564	0.13661	0.16686	0.16697	0.16612	0.18561	0.18896	0.19337	0.19402	0.19426	0.19429	0.19429	0.19429	0.19429	0.19429
Ω_3	0.20255	0.20442	0.25074	0.25106	0.24748	0.27713	0.28158	0.28798	0.28894	0.28927	0.28933	0.28933	0.28933	0.28933	0.28933
$p=5$															
Ω_1	0.068001	0.068022	0.068022	0.068298	0.079443	0.079496	0.084129	0.087611	0.088741	0.089276	0.089442	0.089475	0.089482	0.089484	0.089484
Ω_2	0.13564	0.13581	0.13581	0.13640	0.15886	0.15849	0.16770	0.17455	0.17677	0.17782	0.17815	0.17821	0.17823	0.17823	0.17823
Ω_3	0.20255	0.20309	0.20313	0.20410	0.23822	0.23645	0.25011	0.26007	0.26330	0.26482	0.26530	0.26539	0.26541	0.26542	0.26542

Table 3: Axisymmetric mode $L/a = 20$.

not negligible. Here only the real part is presented. The reason for this specific behavior and the non monotonic convergence pattern have not been clarified.

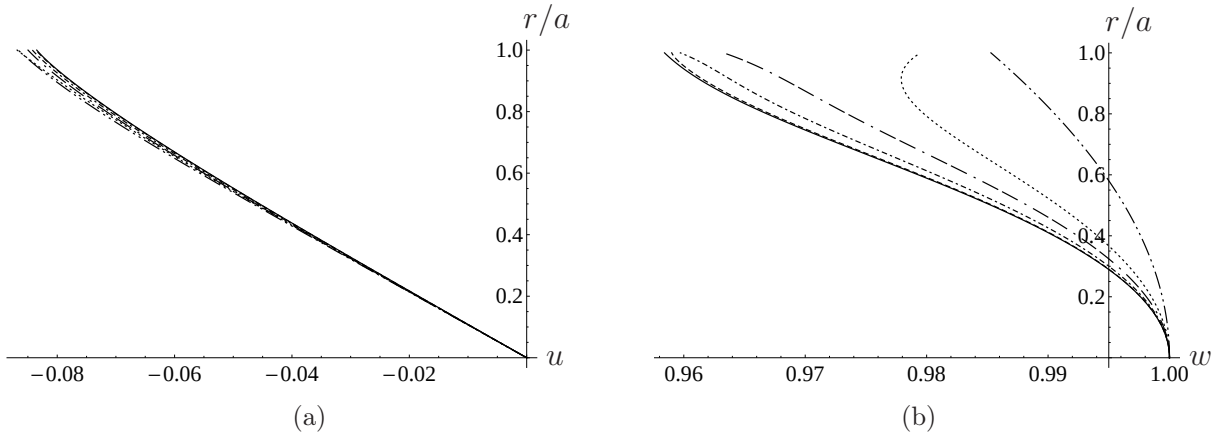

Figure 2: Displacements u (a) and w (b) for the first axisymmetric mode with $p = 5$: —— $N = 150$, - - - $N = 50$, - · - $N = 25$, – – · – – $N = 15$, · · · $N = 10$, – · · – $N = 5$.

The mode shapes for the lowest eigenmode at $z = L/2$ for $p = 5$ are illustrated in Figure 2. Here, the eigenmodes are normalized so that the maximal longitudinal displacement w is equal to unity at the center $r = 0$ and $z = L/2$. The differences among the truncation orders for the almost linear variation of the radial displacement u are rather small, Figure 2(a), while the longitudinal displacement w shows more pronounced variations, Figure 2(b). As for the stress distributions given in Figures 3 and 4, the normal stresses in Figure 3 show in both cases a similar pattern for the different approximations. Clearly, higher order truncations are needed to capture the behaviour close to the surface. The different truncations show more variation in Figure 4, albeit all orders fulfil the free surface boundary condition. Similar to the torsional case for $\sigma_{r\theta}$ the lowest presented order $N = 5$ is close

	$N=2$	$N=3$	$N=4$	$N=5$	$N=6$	$N=10$	$N=15$	$N=25$	$N=35$	$N=50$	$N=70$	$N=90$	$N=110$	$N=130$	$N=150$
$p=1$															
Ω_1	0.18244	0.20782	0.21520	0.22398	0.22398	0.23288	0.23403	0.23421	0.23421	0.23421	0.23421	0.23421	0.23421	0.23421	0.23421
Ω_2	0.36011	0.43827	0.41847	0.44429	0.44949	0.46001	0.46191	0.46225	0.46226	0.46226	0.46226	0.46226	0.46226	0.46226	0.46226
Ω_3	0.52552	0.66914*	0.60308	0.64155	0.68172	0.67212	0.67403	0.67447	0.67448	0.67448	0.67448	0.67448	0.67448	0.67448	0.67448
$p=2$															
Ω_1	0.13661	0.17339	0.17398	0.18825	0.18852	0.20143	0.20677	0.20835	0.20857	0.20860	0.20860	0.20860	0.20860	0.20860	0.20860
Ω_2	0.27071	0.34972	0.35306	0.36862	0.36903	0.39546	0.40717	0.40962	0.41009	0.41014	0.41015	0.41015	0.41015	0.41015	0.41015
Ω_3	0.39918	0.54134	0.56307	0.53236	0.52988	0.56947	0.59224	0.59309	0.59403	0.59403	0.59404	0.59404	0.59404	0.59404	0.59404
$p=3$															
Ω_1	0.13564	0.13661	0.16686	0.16697	0.16612	0.18561	0.18896	0.19337	0.19402	0.19426	0.19429	0.19430	0.19430	0.19430	0.19430
Ω_2	0.26828	0.27157	0.33552	0.33614	0.32667	0.36704	0.37177	0.37982	0.38108	0.38148	0.38155	0.38156	0.38156	0.38156	0.38156
Ω_3	0.39411	0.40218	0.51590	0.51378	0.47525	0.53885	0.54001	0.54930	0.55103	0.55153	0.55161	0.55162	0.55162	0.55162	0.55162
$p=5$															
Ω_1	0.13564	0.13581	0.13581	0.13640	0.15886	0.15849	0.16770	0.17455	0.17677	0.17782	0.17815	0.17821	0.17823	0.17823	0.17823
Ω_2	0.26828	0.26952	0.26969	0.27116	0.31755	0.31278	0.33061	0.34330	0.34739	0.34932	0.34993	0.35005	0.35008	0.35008	0.35008
Ω_3	0.39411	0.39767	0.39918	0.40217	0.47645	0.45771	0.48205	0.49821	0.50335	0.50577	0.50654	0.50670	0.50673	0.50674	0.50674

Table 4: Axisymmetric mode $L/a = 10$.

to zero for all r in the shear stress σ_{rz} in Figure 4(b).

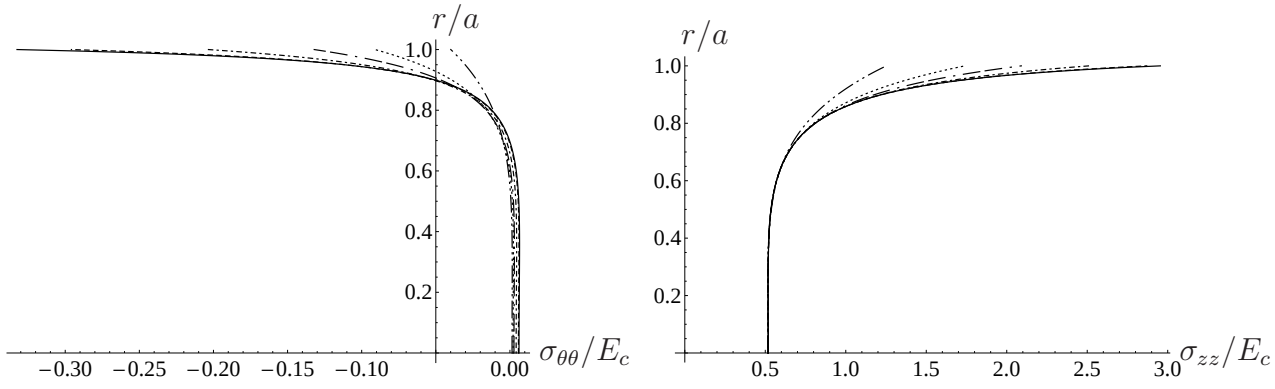

Figure 3: Normal stresses $\sigma_{\theta\theta}$ (a) and σ_{zz} (b) for the first axisymmetric mode with $p = 5$: —— $N = 150$, - - - $N = 50$, - · - $N = 25$, – – · – – $N = 15$, · · · $N = 10$, – · · · – $N = 5$.

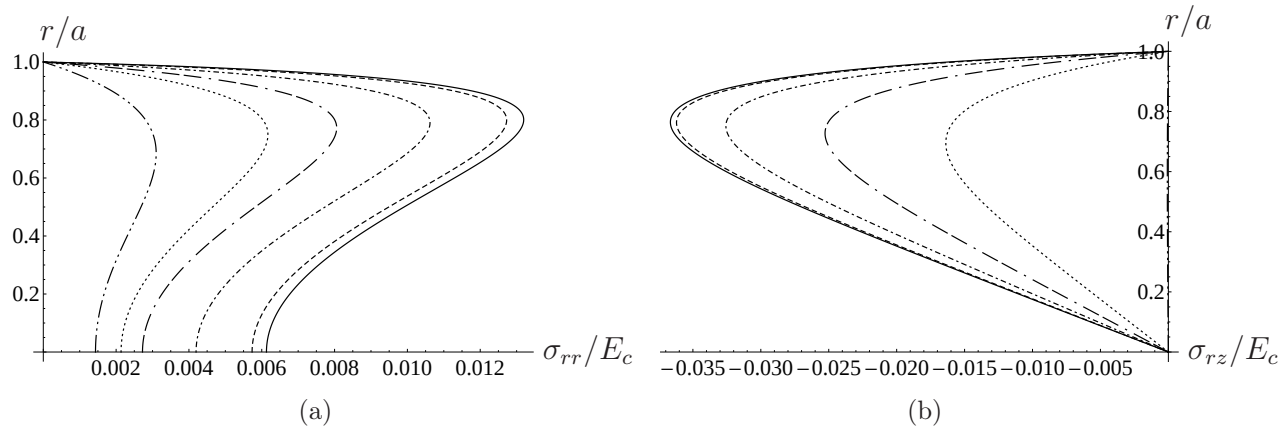

Figure 4: Normal stress σ_{rr} (a) and shear stress σ_{rz} (b) for the first axisymmetric mode with $p = 5$: —— $N = 150$, - - - $N = 50$, -·- $N = 25$, – – · – – $N = 15$, · · · $N = 10$, – · · – $N = 5$.

5.4. Flexural mode, $m = 1$

For the flexural case, there is a coupling between all the displacement fields for that Fourier mode. From Eqs. (3)–(4) the displacements become

$$\begin{aligned} u(r,\theta,z,t) &= \sum_{k=0}^{\infty} r^k u_{k,1}(z,t)\cos\theta, \\ v(r,\theta,z,t) &= \sum_{k=0}^{\infty} r^k v_{k,1}(z,t)\sin\theta, \\ w(r,\theta,z,t) &= \sum_{k=0}^{\infty} r^{k+1} w_{k+1,1}(z,t)\cos\theta. \end{aligned} \tag{35}$$

The equations of motion for flexural motion are obtained from the free lateral surface conditions $\tilde{\sigma}_{rr,1}(a,z,t) = \tilde{\sigma}_{r\theta,1}(a,z,t) = \tilde{\sigma}_{rz,1}(a,z,t) = 0$ from Eqs. (8), (11) and (12). As $v_{0,1} = -u_{0,1}$ from Eqs. (14) and (15) separately, all higher order fields are to be expressed in terms of $u_{0,1}$, $v_{1,1}$, and $w_{1,1}$ using the recursion relations Eqs. (14)–(16). Regarding the end conditions, these become $u_{i,1}(z,t) = v_{i,1}(z,t) = 0$ and $\sigma_{zz,\{1,i\}}(z,t) = 0$ for all i on $z = \{0, L\}$.

In line with the previous torsional and axisymmetric cases, the three lowest eigenfrequencies for various power indexes p and truncations orders N using the length to radius relation $L/a = 20$ and $L/a = 10$ are presented in Tables 5 and 6.

As expected the eigenfrequencies for each frequency order Ω_i in this case are lower than the corresponding ones in the previous cases in Tables 1–4. The convergence rate resembles the axisymmetric case presented in Tables 3 and 4. In this flexural case, the discrepant values for $N = 3$ for indexes $p = 2$ and up are notable. Besides that, the convergence errors generally decrease in a monotonic manner when increasing the power order N.

	$N=3$	$N=4$	$N=5$	$N=6$	$N=10$	$N=15$	$N=25$	$N=35$	$N=50$	$N=70$	$N=90$	$N=110$	$N=130$	$N=150$
$p=1$														
Ω_1	0.0056907	0.0077063	0.0085668	0.0091235	0.0099245	0.010083	0.010109	0.010110	0.010110	0.010110	0.010110	0.010110	0.010110	0.010110
Ω_2	0.022106	0.029768	0.033026	0.035132	0.038132	0.038726	0.038823	0.038826	0.038826	0.038826	0.038826	0.038826	0.038826	0.038826
Ω_3	0.047600	0.063607	0.070356	0.074729	0.080881	0.082098	0.082296	0.082301	0.082301	0.082301	0.082301	0.082301	0.082301	0.082301
$p=2$														
Ω_1	0.0052852	0.0051407	0.0071232	0.0071795	0.0085067	0.0089888	0.0091670	0.0091900	0.0091939	0.0091942	0.0091942	0.0091942	0.0091942	0.0091942
Ω_2	0.020483	0.019965	0.027493	0.027661	0.032671	0.034476	0.035139	0.035225	0.035239	0.035240	0.035240	0.035240	0.035240	0.035240
Ω_3	0.043962	0.042972	0.058659	0.058869	0.069257	0.072956	0.074302	0.074476	0.074505	0.074507	0.074507	0.074507	0.074507	0.074507
$p=3$														
Ω_1	0.0061939	0.0043454	0.0051819	0.0072282	0.0074864	0.0082888	0.0085076	0.0085883	0.0086103	0.0086137	0.0086140	0.0086140	0.0086140	0.0086140
Ω_2	0.023743	0.016902	0.020224	0.027764	0.028795	0.031786	0.032610	0.032911	0.032992	0.033005	0.033006	0.033006	0.033006	0.033006
Ω_2	0.050232	0.036442	0.043826	0.058870	0.061161	0.067251	0.068949	0.069563	0.069726	0.069752	0.069754	0.069754	0.069754	0.069754
$p=5$														
Ω_1	0.0061939	0.0052746	0.0052860	0.0045897	0.0066410	0.0072050	0.0076422	0.0077876	0.0078575	0.0078793	0.0078838	0.0078848	0.0078850	0.0078850
Ω_2	0.023743	0.020325	0.020487	0.017902	0.025573	0.027689	0.029326	0.029869	0.030130	0.030212	0.030228	0.030232	0.030233	0.030233
Ω_3	0.050232	0.043278	0.043968	0.038758	0.054403	0.058750	0.062099	0.063209	0.063741	0.063908	0.063942	0.063949	0.063951	0.063951

Table 5: Flexural mode $L/a = 20$.

	$N=3$	$N=4$	$N=5$	$N=6$	$N=10$	$N=15$	$N=25$	$N=35$	$N=50$	$N=70$	$N=90$	$N=110$	$N=130$	$N=150$
$p=1$														
Ω_1	0.022106	0.029768	0.033026	0.035132	0.038132	0.038726	0.038823	0.038823	0.038823	0.038823	0.038823	0.038823	0.038823	0.038823
Ω_2	0.080195	0.10628	0.11711	0.12418	0.13403	0.13597	0.13628	0.13629	0.13629	0.13629	0.13629	0.13629	0.13629	0.13629
Ω_3	0.15984	0.20880	0.22791	0.24065	0.25860	0.26210	0.26266	0.26267	0.26267	0.26267	0.26267	0.26267	0.26267	0.26267
$p=2$														
Ω_1	0.020483	0.019965	0.027493	0.027661	0.032671	0.034476	0.035139	0.035225	0.035239	0.035240	0.035240	0.035240	0.035240	0.035240
Ω_2	0.073790	0.072349	0.097804	0.097853	0.11468	0.12059	0.12272	0.12299	0.12304	0.12304	0.12304	0.12304	0.12304	0.12304
Ω_3	0.14595	0.14389	0.19094	0.18964	0.22086	0.23159	0.23529	0.23577	0.23585	0.23586	0.23586	0.23586	0.23586	0.23586
$p=3$														
Ω_1	0.023743	0.016902	0.020224	0.027764	0.028795	0.031786	0.032610	0.032911	0.032992	0.033005	0.033006	0.033006	0.033006	0.033006
Ω_2	0.083076	0.061443	0.074350	0.097538	0.10148	0.11115	0.11386	0.11484	0.11510	0.11513	0.11514	0.11514	0.11514	0.11514
Ω_3	0.16014	0.12229	0.15011	0.18840	0.19622	0.21343	0.21826	0.22000	0.22043	0.22050	0.22050	0.22050	0.22050	0.22050
$p=5$														
Ω_1	0.023743	0.020325	0.020487	0.017902	0.025573	0.027689	0.029326	0.029869	0.030130	0.030212	0.030228	0.030232	0.030233	0.030233
Ω_2	0.083076	0.072009	0.073795	0.065663	0.090438	0.097389	0.10272	0.10448	0.10533	0.10559	0.10565	0.10566	0.10566	0.10566
Ω_3	0.16014	0.13998	0.14594	0.13204	0.17557	0.18806	0.19754	0.20065	0.20214	0.20260	0.20270	0.20272	0.20272	0.20272

Table 6: Flexural mode $L/a = 10$.

The mode shapes u and v for the lowest eigenmode at $z = L/2$ for $p = 5$ are illustrated in Figure 5. In this case, the eigenmodes are normalized so that the maximal radial displacement u is equal to unity at $r = a$ and $z = L/2$. The variation among the different truncation orders are more pronounced for v in Figure 5(b) compared to u in Figure 5(a). As for the longitudinal displacement w the displacement varies almost linearly for all truncation orders with small differences among the different orders; this result is not displayed here.

As for the normal stress distributions given in Figure 6, these results resemble the axisymmetric ones in Figure 3, albeit that Figure 6(b) is even more similar to the shape of $\sigma_{\theta z}$ for the torsional case in Figure 1(b). The rest of the stresses are displayed in Figures 7 and 8. As before, all orders fulfil the free surface boundary condition in Figures 7 and 8(a).

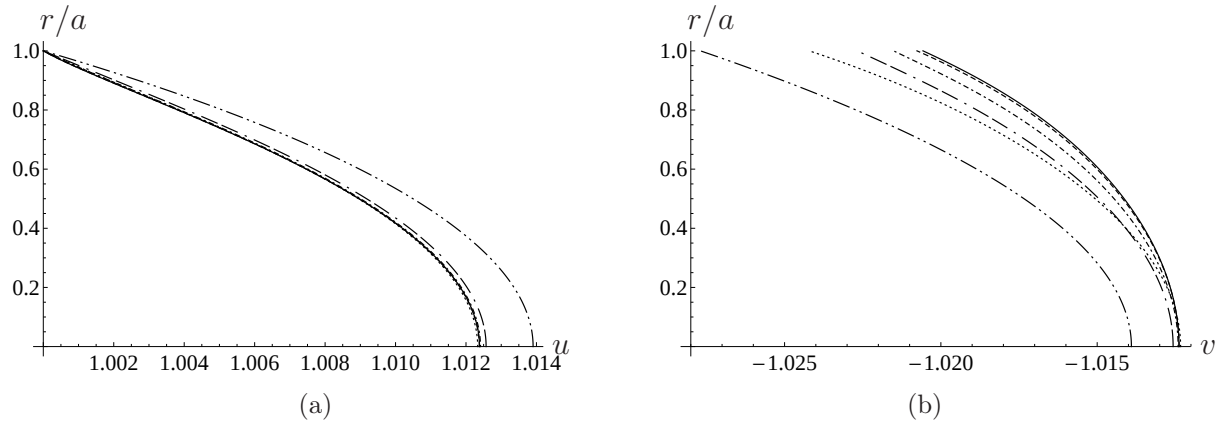

Figure 5: Displacements u (a) and v (b) for the first flexural mode with $p = 5$: —— $N = 150$, - - - $N = 50$, -·- $N = 25$, – – · – – $N = 15$, · · · $N = 10$, – · · · – $N = 5$.

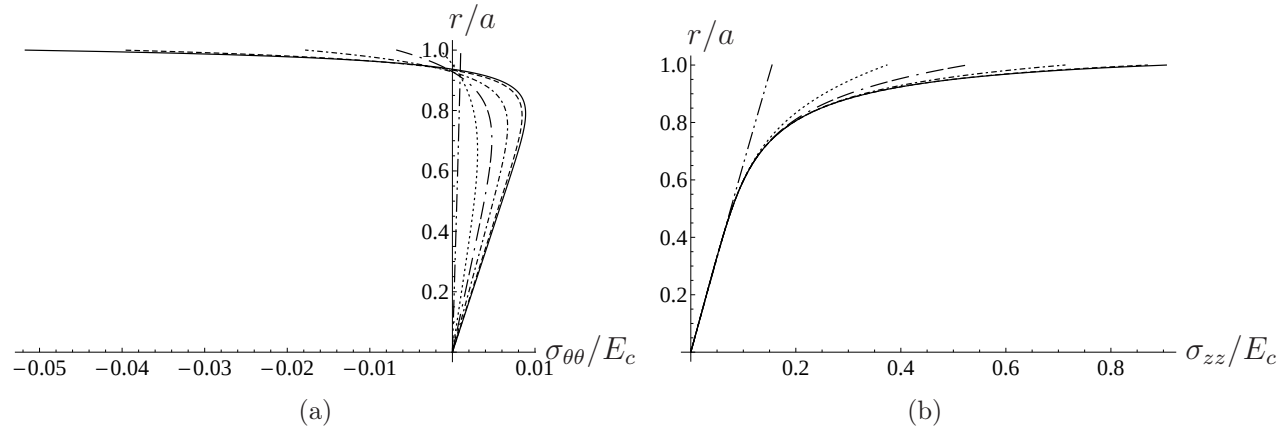

Figure 6: Normal stresses $\sigma_{\theta\theta}$ (a) and σ_{zz} (b) for the first flexural mode with $p = 5$: —— $N = 150$, - - - $N = 50$, -·- $N = 25$, – – · – – $N = 15$, · · · $N = 10$, – · · · – $N = 5$.

5.4.1. Comparison to beam theory

In order to validate the presented results, comparisons are to be performed with results from the literature. There are, to our knowledge, very few eigenfrequency results reported for FG solid cylinders for any of the various modes considered herein (torsional, axisymmetric and flexural motion). However, one such case is the eigenfrequency results for FG beams studied by Huang and Li [20] using a Timoshenko like theory. Table 7 illustrates some of the results reported in [20], denoted HL, together with the corresponding mode results using the present theory for a few of the lower truncations orders as well as high order. The material phases used in [20] are aluminum and zirconia, where the ceramic radial distribution follows from Eq. (29), while the material parameter variations are modeled using the Voigt model.

It is clear from the results that the Timoshenko like theory [20] (using methods based on integration over the cross section) render similar or better results than the present lowest

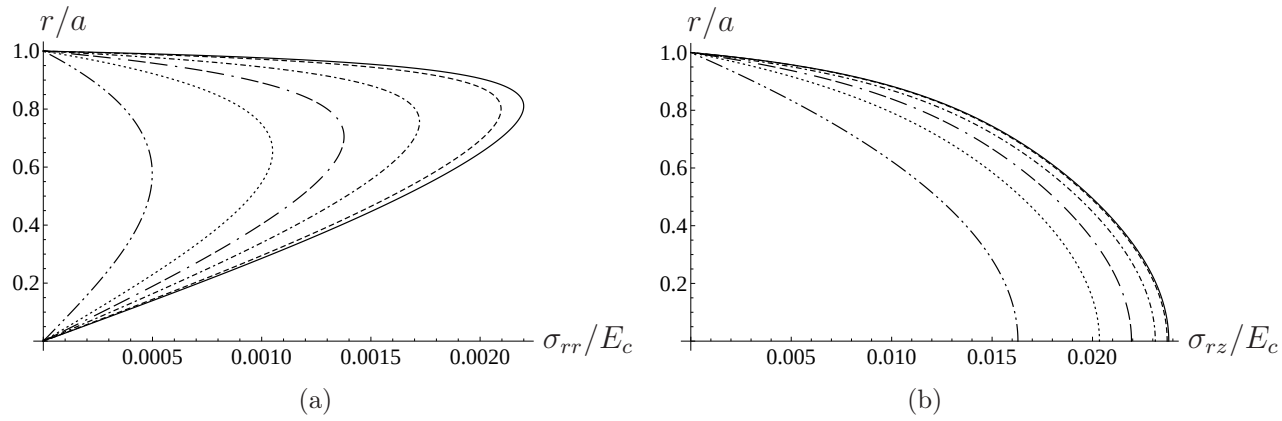

Figure 7: Normal stress σ_{rr} (a) and shear stress σ_{rz} (b) for the first flexural mode with $p = 5$: —— $N = 150$, - - - $N = 50$, - · - $N = 25$, – – · – – $N = 15$, · · · $N = 10$, – · · – $N = 5$.

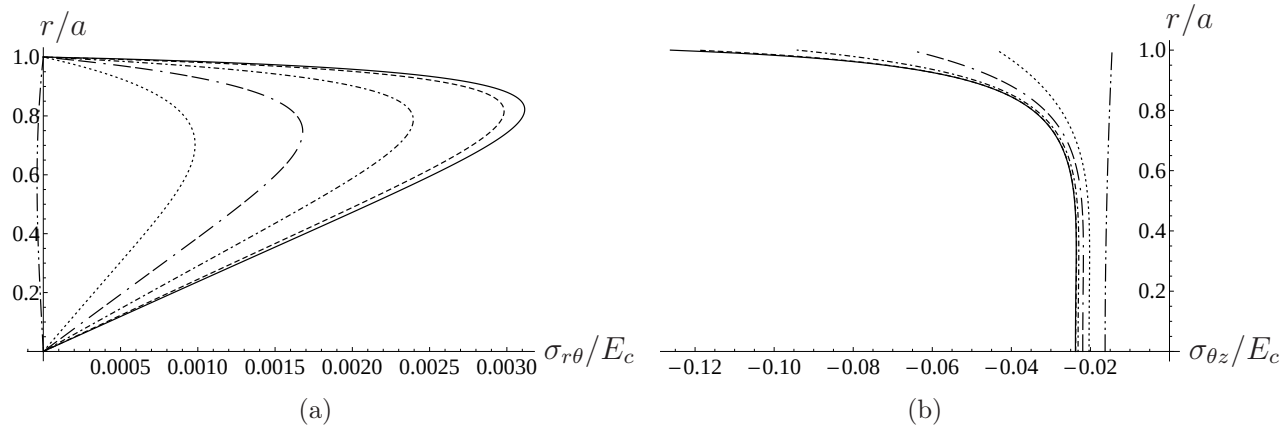

Figure 8: Shear stress $\sigma_{r\theta}$ (a) and shear stress $\sigma_{\theta z}$ (b) for the first flexural mode with $p = 5$: —— $N = 150$, - - - $N = 50$, - · - $N = 25$, – – · – – $N = 15$, · · · $N = 10$, – · · – $N = 5$.

order theories (using term by term series expansion of the governing 3D equations). The $N = 3$ results are very similar to HL for $p = 5$, while being inferior for $p = 1$. The $N = 5$ case is of the same accuracy order as the HL case. A similar accuracy behavior was presented in the homogeneous beam case [41]. It could be noted that the present series expansion theories always fulfil the homogeneous boundary conditions (to all orders), which is not generally the case for Timoshenko like theories.

6. Conclusion

This work considers a hierarchy of dynamic equations for solid isotropic functionally graded circular cylinders. The FG material is such that the density and the Lamé parameters are assumed to vary in the radial direction. The adopted approach starts from the three dimensional elastodynamic theory using Fourier expansions in the circumferential direction

	HL	$N=3$	$N=5$	$N=150$
$p=1$				
Ω_1	0.0481	0.0348	0.0445	0.0462
Ω_2	0.170	0.127	0.158	0.164
Ω_3	0.329	0.253	0.306	0.318
$p=5$				
Ω_1	0.0472	0.0471	0.0406	0.0441
Ω_2	0.165	0.165	0.146	0.156
Ω_3	0.318	0.318	0.290	0.303

Table 7: Flexural mode $L/a = 10$ using theory due to Huang and Li (HL) [20] and present theory for different truncations order.

and power series expansions in the radial direction. A hierarchy of variationally consistent partial differential equations and pertinent end boundary conditions are obtained for FG cylinders for different circumferential orders.

The three lowest eigenfrequencies are calculated for torsional, axisymmetric and flexural modes for different FG constitutions. In each case the highest presented truncation order is such that the corresponding eigenfrequency calculation has converged. Hence, this shows that these higher order theories may act as benchmark solutions in line with the results for plates [43] and shells [8] using similar approach. For the lower order expansions, these equations may act as simpler engineering cylinder equations. It is seen here that modest to high order truncations are in most cases required to render results that are of adequate accuracy. This differs to the homogeneous cylinder case studied in [40, 41] where low to modest order truncations are sufficient. There are also significant differences between homogeneous and FG cylinders regarding the mode shapes and stress distributions for the first mode in each case (torsional, axisymmetric, flexural). It should be stressed that although the presented benchmark solutions have not been confirmed correct, the corresponding eigenfrequency results in the special case of homogeneous structures are in line with the 3D results presented in the literature [40, 41].

Possible extension on the present work is to study FG cylinders where the material properties vary in circumferential or longitudinal directions. The fundamentals for such formulations may be developed using methods similar to the ones outlined in the present paper, but the systematic organization and solutions of such equations may differ considerably to the present work. Preliminary results for the circumferential case show that sets of cylinder equations are readily obtained, albeit the various circumferential orders couple in a non trivial manner. Hopefully this issue will be resolved in the near future.

Acknowledgement

This research did not receive any specific grant from funding agencies in the public, commercial, or not-for-profit sectors.

References

[1] Birman V, Byrd LW. Modeling and analysis of functionally graded materials and structures. Appl Mech Rev 2007;60:195–216.

[2] Shen HS. Functionally graded materials: nonlinear analysis of plates and shells. CRC Press, 2009.

[3] Loy CT, Lam KY, Reddy JN. Vibration of functionally graded cylindrical shells. Int J Mech Sci 1999;41:309–324.

[4] Zhao X, Lee YY, Liew KM. Thermoelastic and vibration analysis of functionally graded cylindrical shells. Int J Mech Sci 2009;51:694–707.

[5] Tornabene F, Viola E, Inman DJ. 2-D differential quadrature solution for vibration analysis of functionally graded conical, cylindrical shell and annular plate structures. J Sound Vib 2009;328:259–290.

[6] Patel BP, Gupta SS, Loknath MS, Kadu CP. Free vibration analysis of functionally graded elliptical cylindrical shells using higher-order theory. Compos Struct 2005;69:259–270.

[7] Batra RC, Iaccarino GL. Exact solutions for radial deformations of a functionally graded isotropic and incompressible second-order elastic cylinder. Int J Nonlin Mech 2008;43:383–398.

[8] Vel SS. Exact elasticity solution for the vibration of functionally graded anisotropic cylindrical shells. Compos Struct 2010;92:2712–2727.

[9] Asghari M, Akhlaghi M. Natural frequency analysis of 2D-FGM thick hollow cylinder based on three-dimensional elasticity equations. Eur J Mech A/Solids 2011;30:72–81.

[10] Pilafkan R, Folkow PD, Darvizeh M, Darvizeh A. Three dimensional frequency analysis of bidirectional functionally graded thick cylindrical shells using a radial point interpolation method (RPIM) Eur J Mech A/Solids 2013;39:26–34.

[11] Fazzolari FA, Carrera E. Refined hierarchical kinematics quasi-3D Ritz models for free vibration analysis of doubly curved FGM shells and sandwich shells with FGM core. J Sound Vib 2014;333:1485–1508.

[12] Thai H-T, Kim S-E. A review of theories for the modeling and analysis of functionally graded plates and shells. Compos Struct 2015;128:70–86.

[13] Dai H-L, Rao Y-N, Dai T. A review of recent researches on FGM cylindrical structures under coupled physical interactions, 2000-2015. Compos Struct 2016;152:199–225.

[14] Sankar BV. An elasticity solution for functionally graded beams. Compos Sci Technol 2001;61:689–696.

[15] Rooney F, Ferrari M. Tension, bending, and flexure of functionally graded cylinders. Int J Solids Struct 2001;38:413–421.

[16] Zhong Z, Yu T. Analytical solution of a cantilever functionally graded beam. Compos Sci Technol 2007;67:481–488.

[17] Li X-F. A unified approach for analyzing static and dynamic behaviors of functionally graded Timoshenko and Euler-Bernoulli beams. J Sound Vib 2008;318:1210–1229.

[18] Aydogdu M, Taskin V. Free vibration analysis of functionally graded beams with simply supported edges. Mater Des 2007;28:1651–1656.

[19] Sina SA, Navazi HM, Haddadpour H. An analytical method for free vibration analysis of functionally graded beams. Mater Des 2009;30:741–747.

[20] Huang Y, Li X-F. Bending and vibration of circular cylindrical beams with arbitrary radial nonhomogeneity. Int J Mech Sci 2010;52:595–601.

[21] Şimşek M. Fundamental frequency analysis of functionally graded beams by using different higher-order beam theories. Nucl Eng Des 1998;210:661–672.

[22] Giunta G, Crisafulli D, Belouettar S, Carrera E. Hierarchical theories for the free vibration analysis of functionally graded beams. Compos Struct 2011;94:68–74.

[23] Thai H-T, Vo TP. Bending and free vibration of functionally graded beams using various higher-order shear deformation beam theories. Int J Mech Sci 2012;62:57–66.

[24] Pradhan KK, Chakraverty S. Free vibration of Euler and Timoshenko functionally graded beams by Rayleigh-Ritz method. Comp B Eng 2013;51:175–184.

[25] Chakraborty A, Gopalakrishnan S, Reddy JN. A new beam finite element for the analysis of functionally graded materials. Int J Mech Sci 2003;45:519–539.

[26] Goupee AJ, Vel SS. Optimization of natural frequencies of bidirectional functionally graded beams. Struct Multidisc Optim 2006;32:473–484.

[27] Su H, Banerjee JR, Cheung CW. Dynamic stiffness formulation and free vibration analysis of functionally graded beams. Compos Struct 2013;106:854–862.

[28] Roque, CMC, Martins, P. Differential evolution optimization for the analysis of composite plates with radial basis collocation meshless method. Compos. Struct. 2015;133:1191–1197.

[29] Fazzolari, FA. Quasi-3D beam models for the computation of eigenfrequencies of functionally graded beams with arbitrary boundary conditions. Compos Struct 2016;154:239–255.

[30] Horgan CO, Chan AM. Torsion of functionally graded isotropic linearly elastic bars. J Elasticity 1999;52:181–199.

[31] Batra RC. Torsion of functionally graded cylinder. AIAA J 2006;44:1363–1365.

[32] Tarn J-Q, Chang H-H. Torsion of cylindrically orthotropic elastic circular bars with radial inhomogeneity: some exact solutions and end effects. Int. J. Solids Struct. 2008;45:303-319.

[33] Barretta R, Feo L, Luciano R. Some closed-form solutions of functionally graded beams undergoing nonuniform torsion. Compos Struct 2015;123:132–136.

[34] Akgöz B, Civalek Ö. Longitudinal vibration analysis of strain gradient bars made of functionally graded materials (FGM). Compos B Eng 2013;55:263–268.

[35] Xue C-X, Pan E. On the longitudinal wave along a functionally graded magneto-electro-elastic rod. Int J Eng Sci 2013;62:48–55.

[36] Hong M, Park I, Lee U. Dynamics and waves characteristics of the FGM axial bars by using spectral element method. Compos Struct 2014;107:585–593.

[37] Dorduncu M, Apalak MK, Cherukuri HP. Elastic wave propagation in functionally graded circular cylinders. Comp B Eng 2015;73:35–48.

[38] Boström A. On wave equations for elastic rods. Z Angew Math Mech 2000;80:245-25.

[39] Achenbach JD. Wave Propagation in Elastic Solids. North-Holland;1973.

[40] Folkow PD, Mauritsson K. Dynamic higher-order equations for finite rods. Q Jl Mech Appl Math 2010;63:1–22.

[41] Abadikhah H, Folkow PD. A hierarchy of dynamic equations for solid isotropic circular cylinders. Wave Motion 2013;51:206–221.

[42] Vel SS, Batra RC. Three-dimensional analysis of transient thermal stresses in functionally graded plates. Int J Solids Struct 2003;40:7181–7196.

[43] Vel SS, Batra RC. Three-dimensional exact solution for the vibration of functionally graded rectangular plates. J Sound Vib 2004;272:703–730.